Alleviation of the Oscillation Behavior in Kundur Benchmark via Fuzzy Based Resistive Braking Scheme Considering Time Latencies and Declined Inertia

Mohamed Fayez[1*], F. Bendary[2], M. El-Hadidy[3], M. Mandor[4]
1- Cairo Electricity Production Company, Cairo, Egypt.
Email: eng_mf69@yahoo.com (Corresponding author)
2- Departmen of Electrical Engineering, Benha University, Cairo, Egypt.
Email: fahmybendary10@gmail.com
3- Egyptian Electricity Holding Company, Cairo, Egypt.
Email: dr_alhadidy@hotmail.com
4- Department of Electrical Engineering, Benha University, Cairo, Egypt.
Email: madel_ibec@yahoo.com

Received: October 2020 Revised: March 2021 Accepted: May 2021

ABSTRACT:
Oscillation behavior is usually experienced in all power grids as an inherent characterization related to their very existence. Inter-area oscillations are considered to be the most likely to jeopardize the synchronous integrity in power grids. They cause declining the quality conditions of the transmitted power which could have adverse impacts on big consumers' load fed directly from the transmission grid. Therefore, the prime target of this investigation is to alleviate the power oscillations resulting from the different grid disturbances. This aim is accomplished by utilizing a fuzzy based resistor braking strategy taking three energization signals into consideration. Additionally, various time latencies are considered to examine and evaluate the propositioned strategy under these conditions. Also, declined inertia situations resulting from the escalated incursion levels of grid-connected photovoltaic plants are considered to examine the propositioned strategy from a futuristic operational perspective. For examining the effectivity of the propositioned strategy, non-linear time-domain simulation studies are conducted on Kundur benchmark via MATLAB/Simulink platform. Five comparative simulation studies of the benchmark after being subjected to variety of perturbations demonstrate the effectivity of propositioned strategy.

KEYWORDS: Dynamic Resistor Braking, Fuzzy Logic Control, Kundur Benchmark Oscillation Behavior.

1. INTRODUCTION

Power systems have been experiencing the oscillation behavior since the very beginning of their modern form [1], [2]. Among the multiple presently conceivable forms of grid oscillating behavior, inter-area oscillations are considered to be the most likely to jeopardize the synchronous integrity in electrical grids because they have a wide frequency range accompanied with inherent poor damping and involve many participant generators spreading throughout large geographical areas [1], [2]. They also cause declining the quality conditions of the transmitted power which could have adverse impacts on big consumers' load fed directly at the transmission voltage levels [3]. Alleviation of these oscillations has been a matter of overwhelming importance in both industry and academia on the account of their serious consequents on the grid [4]. Inter-area oscillations curtail the power transferring capacity of a transmission interfaces and jeopardize the operational security of the power networks by being the prime culprit for many worldwide blackouts [4], [5]. The poor damping action related to these oscillations leaves open a wide range of possibilities for cascading blackout [6], [7]. Blackouts have annihilating consequences on countries measured in the terms of massive economic damages and potential human casualties [6], [7]. Therefore, the prime objective of this investigation is the alleviation of inter-area oscillatory behavior developed as an outcome to the different disturbances.

To lower the probabilities of blackouts related to inter-area oscillatory behavior, the damping related to these oscillations must be boosted [1], [2]. Among the participating sources of the grid natural damping is the

Paper type: Research paper
DOI: https://doi.org/10.52547/mjee.15.4.27
How to cite this paper: M. Fayez, F. Bendary, M. El-Hadidy and M. Mandor, **"Alleviation of the Oscillation Behavior in Kundur Benchmark via Fuzzy Based Resistive Braking Scheme Considering Time Latencies and Declined Inertia"**,Majlesi Journal of Electrical Engineering, Vol. 15, No. 4, pp. 27-41, 2021.

electrical grid loading burdens [2]. Thus, if the network loading level is momentarily increased, just for a little bit, to allow for the excess energy to be properly dissipated and hence the energy equity is restored and maintained, adds supplementary positive damping to the network natural damping. One approach to accomplish this task is the employment of dynamic resistive braking strategies.

The strategy of dynamic resistive braking in electrical grids is simply relying on the energization of an artificial load banks if the grid is accelerating as a direct result to nearby faults and after the energy equity is maintained or if the grid is decelerating, the load bank will be deenergized [8]. Dynamically controlled resistor brakes have been subject of decades of development research in the fields of transient stability enhancement since the early sixties [8].

In 1960, British Columbia (B.C.) hydro and power authority commissioned and installed cast iron 600 MW shunt connected resistor brake near Peace River (230×10) MW hydro power plant [9]. The brake was linked to the 500 kV Peace River transmission grid via 500:132 kV step-down transformer located at Portage Mountain substation [9]. It was the first large-scale resistor brake installations in USA for the benefit of increasing the first swing stability limit of Peace River transmission system [9]. The power utility of Bonneville USA, has commissioned and installed stainless steel 1400 MW resistor brake at Chief Joseph substation in the Western Interconnection in 1973 [10]. The brake was linked to the grid via 500:240 kV step-down transformer [10].

This article contributes to the academic peer community in what follows:

- Proposing a fuzzy based resistor brake for alleviation of the oscillations in the transmitted power in Kundur benchmark with three distinct energization signals,
- Considering various communication latencies in the propositioned strategy and determining the delay threshold beyond which the propositioned strategy is ineffective,
- Considering declined inertia conditions in the studied benchmark and examining the propositioned strategy under these situations.

The other sections of this work are structured as following. In the second section, modelling of the different benchmark components is presented. In the third section, a briefing on fuzzy controllers is given. In the fourth section, a briefing of the studied benchmark is presented in company with the comparative 10-seconds simulation results in the time domain. In the fifth section, the key conclusions of this investigation are presented. Finally, the list of references utilized in this investigation and the data tables of the benchmark are introduced.

2. SYSTEM MODELLING

To indicate the effectivity of the propositioned alleviation strategy, Kundur benchmark is selected in this investigation. All the benchmark elements are selected from MATLAB/Simulink library. All the bulk loads are modelled as a constant PQ load. Throughout the simulation studies presented within this paper, transmission grid is modelled utilizing the medium π-model, and the lumped distributed parameter model. From practical perspective, the control signals utilized to help a FACTS controller mitigate the oscillations take some time to reach the FACTS location. The energization signal time latency (τ) is expressed as $F(s) = e^{-\tau s}$ as the work introduced in [7].

2.1. Generator Model

The modelling of the generator is in detail, as sixth−order (full) model, considering static exciter because of its wide spread appearance in modern power grids. The equations describing the behavior of synchronous machine as a full model incorporating the leakage reactances and neglecting damping are as the following [11]:

$$\frac{d}{dt}E'_d = \frac{1}{T'_q}\left[\left(-E'_d + (X_q - X'_q)\left\{I_q - \frac{X'_q - X''_q}{(X''_q - X_l)^2}(\psi_q + I_q(X'_q - X_l) - E'_d\right\}\right)\right] \quad (1)$$

$$\frac{d}{dt}E'_q = \frac{1}{T'_d}\left[\left(-E'_q - (X_d - X'_d)\left\{I_d - \frac{X'_d - X''_d}{(X''_d - X_l)^2}(\psi_d + I_d(X'_d - X_l) - E'_q\right\} + E_{fd}\right)\right] \quad (2)$$

$$\frac{d}{dt}\psi_d = \frac{1}{T''_d}\left[E'_q - I_d(X'_d - X_l) - \psi_d\right] \quad (3)$$

$$\frac{d}{dt}\psi_q = \frac{1}{T''_q}\left[E'_d - I_q(X'_q - X_l) - \psi_q\right] \quad (4)$$

$$\frac{d}{dt}\Delta\omega_1 = \frac{1}{2H}[P_m - P_e] \quad (5)$$

$$\frac{d}{dt}\delta_1 = [\omega_1 - \omega_{syn}] \quad (6)$$

The generator per-unit (p.u.) air gap electrical torque equation is [11]:

$$T_e = \psi_d i_q - \psi_q i_d \quad (7)$$

All generators are equipped with IEEE ST1A type static exciters. The exciter parameters are quoted from [12].

2.2. Resistor brake model

A resistor brake linked to the grid through an AC-to-AC voltage controller is given the acronym 'TCBR' for thyristor controlled braking resistor [12]. TCBR is a special purpose FACTS element [12]. TCBR is special FACTS because it is implemented in dealing with particular problems [12]. Resistor brake strategy was proposed in [13], to alleviate the torsional and inertial

oscillatory modes of steam turbogenerator implementing the speed deviation signals from both of the alternator and the prime mover as control signals. In [14], the researcher suggested TCBR strategy based on traditional minimum-time and artificial intelligence strategies to alleviate the subsynchronous resonance (SSR) oscillations using the alternator speed deviation and its derivative as control signals.

In [15], the researchers proposed TCBR strategy based upon a fuzzy approach to improve the first swing stability margin of multimachine power grid. While in [16], the researchers proposed TCBR strategy based upon a fuzzy system accompanied with the optimum selection of autoreclosing time for circuit breakers to prevent the first swing instabilities of power grids under failed autoreclosing operations. In [17], the researchers suggested global TCBR strategy based upon fuzzy system to improve the pot-contingency stability margin in a multi-machine power grid considering time delay. While in Ref. [18], the researchers presented a fuzzy based switching technique for TCBR accompanied with coordinating operation of SVC to ameliorate the transient performance of electrical networks. Also, in [19], the researcher introduced resistor brake strategy based on reinforcement learning for enhancing the network stability responses after the various grid contingencies. In [20], a coordinating operation of excitation system control, prime mover control, and resistor brake strategy to ameliorate the transient and steady state stabilities of power grids was presented. In paper [21], the researcher presented centralized resistor brake strategy accompanied with coordinating operation of STATCOM to ameliorate the first-swing stability of network-interconnected wind park. For elucidation benefits, Fig. 1 exhibits the representing of the resistive braking strategy under consideration.

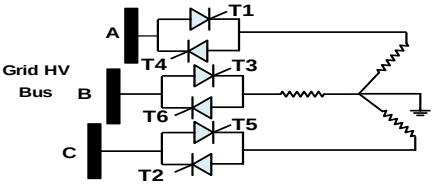

Fig. 1. Grid-connected TCBR installation.

Each phase of a TCBR contains two high-power thyristors, in back-to-back connection, connected with linear resistance element [12].

3. FUZZY LOGIC CONTROLLER (FLC)

It is a rule-based controller of nonlinear type that predicates on the exploitation of the expert knowledge [22]. FLCs introduce superior performance levels by exploitation the expert's knowledge conception in treating unlimited variety of multidisciplinary control issues [22]. The elementary configuration of generic FLC is typically comprised of the four primary stages: fuzzification, knowledge base, inference engine, and defuzzification which is graphically supported by Fig. 2 [22]. The fuzzification stage is responsible for mapping the nonfuzzy inputs into fuzzy variables by using normalized Membership Functions (MFs) and irregularly input weighting factors [22]. It is simply a rule activation process [22]. In the sequent stage, the inference engine satisfactorily determines the reasonable outputs in accordance with the embedded fuzzy rules written by the fuzzy system designers [22]. Eventually, the defuzzification step is responsible for converting the fuzzy outputs into nonfuzzy values by using normalized MFs and irregularly output weighting factors [22].

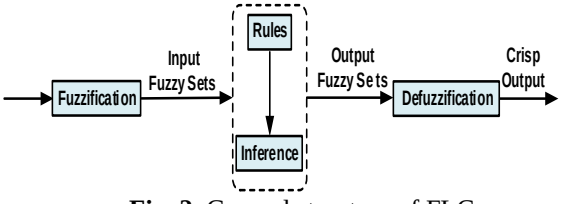

Fig. 2. General structure of FLC.

Defuzzification is simply a mathematical averaging function and it is the union of all the rule consequences of the embedded fuzzy rules [23], [24]. The defuzzification procedures, mainly in FLC with Mamdani type, represent heavy computational burdens in real life fuzzy applications [24]. Takagi-Sugeno (TS) controllers do not require defuzzification since the involved MFs for the output are either a linear function or constant value, i.e. numerically represented, which makes the TS controllers more efficient than Mamdani controllers from the computational perspective [23], [24]. The aggregated output of all TS rules is achieved either via "weighted average," or "weighted sum" operators which makes the time-consuming defuzzification process avoidable.

FLCs have been long exploited to deal with many issues in electrical grids such as, alleviating the different forms of grid oscillation behavior, future load predicting, various fault diagnosing, grid stability improving, alternator predictive maintenance scheduling, and detecting the highly resistive short circuits in the grid [12].

4. TEST SYSTEM DESCRIPTION AND SIMULATION RESULTS

A Schematic diagram of studied system is depicted in Fig. 3 [25]. It is a four machine eleven bus two-area power system model. It is a hypothetical grid with realistic parameters and it is widely employed for studying grid oscillation behavior for the last two decades or so [25]. The benchmark was carefully designed to conduct a comprehensive Eign analysis for

thoroughly understanding the different aspects of this problem [25]. The turbine operates at 3600 rpm. The base system has two similar areas (active networks) connected via 220 Km 230 kV double tie lines which makes the transmission interface relatively weak [25]. Two identical 900 MVA synchronous generators driven by steam turbines are involved in each area. For brevity reasons, the dynamic data for the benchmark are obtained from [25]. All the four turbogenerators have the same MVA rating, terminal voltage rating, time constants and electrical parameters. There is large degree of similarity with the sole discrepancy that is the inertia constant. Three low frequency electro-mechanical oscillatory modes exist in the benchmark, two local modes, one in each area, and one inter-area mode and they are often stimulated simultaneously [25]. Real power crossing the interconnecting transmission corridor is manipulated by changing the load banks at the load busses.

An electric power transaction of 413 MW is exported from generation-rich area 1 to area 2 which is happened to be suffering from shortage in generation during the steady state operation.

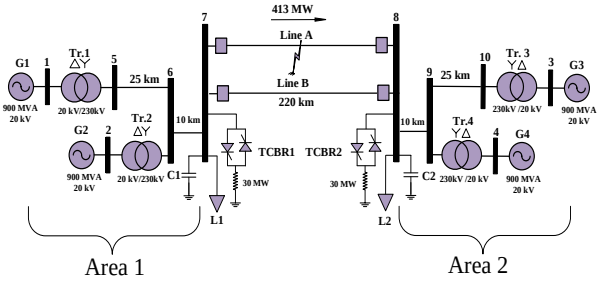

Fig. 3. Kundur test system with double 30 MW TCBRs.

Each area contains a 30 MW TCBR which are installed at the two terminals of the interconnecting transmission interface, i.e. at bus 7 and at bus 8, as pictured in Fig. 3. Each TCBR is controlled via a dedicated FLC. The necessity of adopting a wide-area based oscillation mitigation approach in electrical grids is relied on the consideration that major electrical infrastructure catastrophic events are associated to dynamic phenomenon having a wide geographical influence such as, inter-area oscillations, voltage, and transient instabilities.

Many global control signals such as Totalized Kinetic Energy Deviation (TKED), and the time derivative of the TKED, are commonly employed as an insertion control signal for the resistor brakes in other applications [15]-[17]. As in [26], the speed of equivalent one-machine infinite bus ($OMIB_{Speed}$) is utilized as a control signal to the FLCs. The relative $OMIB_{Speed}$ signals are obtained as follows:

$$\omega_{Area1} = \frac{1}{H_1+H_2}[\omega_1 H_1 + \omega_2 H_2] \quad (8)$$

$$\omega_{Area2} = \frac{1}{H_3+H_4}[\omega_3 H_3 + \omega_4 H_4] \quad (9)$$

$$OMIB_{Speed1} = \omega_{Area1} - \omega_{Area2} \quad (10)$$

$$OMIB_{Speed2} = \omega_{Area2} - \omega_{Area1} \quad (11)$$

Where, ω_{Area1} is the equivalent speed of area 1, ω_{Area2} is the equivalent speed of area 2, $OMIB_{Speed1}$ is speed of area 1 with respect to (w.r.t.) area 2, and $OMIB_{Speed2}$ is speed of area 2 w.r.t. area 1.

Then the power that should be consumed via each TCBR predicates on the $OMIB_{Speed}$. Therefore, if ω_{Area1} is greater than ω_{Area2} then the $OMIB_{Speed1}$ is positive and area 1 has more kinetic energy than area 2 which necessitates the energization of $TCBR_1$ to preserve the energy equity among the two areas. Quite the contrary, if ω_{Area2} is greater than ω_{Area1} then the $OMIB_{Speed2}$ is positive and area 2 has more kinetic energy than area 1 which necessitates the energization of $TCBR_2$ to preserve the energy equity among the two areas. And if ω_{Area1} is equal ω_{Area2} then there will be no need for energizing the TCBR.

Also, the Relative Kinetic Energy Deviation (RKED) among both areas is also considered as an input energization signal to the FLCs. the RKED for each area is determined by calculating the Kinetic Energy Deviation (KED_i) for each machine in joule as per the expression:

KED_i = (machine kinetic energy at transient state) − (machine kinetic energy at steady state)

Or

$$KEDi = \frac{1}{2}J_i\omega_i^2 - \frac{1}{2}J_i\omega_o^2 \qquad joule \quad (12)$$

Where, J_i denotes the shaft inertia of machine i (in Kg. m^2), ω_i is the speed of machine i (in mechanical rad/s), and ω_o is synchronous angular speed in (mechanical rad /s). Throughout this chapter, i=1, 2, 3, and 4 are denoting the machine number in Kundur benchmark.

Then the RKED for area 1

($RKED_1$) = TKED for area (1) − TKED for area (2)

Or

$$RKED_1 = \left[\left(\frac{1}{2}J_1\omega_1^2 - \frac{1}{2}J_1\omega_o^2\right) + \left(\frac{1}{2}J_2\omega_2^2 - \frac{1}{2}J_2\omega_o^2\right)\right] - \left[\left(\frac{1}{2}J_3\omega_3^2 - \frac{1}{2}J_3\omega_o^2\right) + \left(\frac{1}{2}J_4\omega_4^2 - \frac{1}{2}J_4\omega_o^2\right)\right] \qquad joule \quad (13)$$

And, the RKED for area 2 ($RKED_2$) = TKED for area (2) −TKED for area (1).

$$RKED_2 = \left[\left(\frac{1}{2}J_3\omega_3^2 - \frac{1}{2}J_3\omega_o^2\right) + \left(\frac{1}{2}J_4\omega_4^2 - \frac{1}{2}J_4\omega_o^2\right)\right] - \left[\left(\frac{1}{2}J_1\omega_1^2 - \frac{1}{2}J_1\omega_o^2\right) + \left(\frac{1}{2}J_2\omega_2^2 - \frac{1}{2}J_2\omega_o^2\right)\right] \qquad joule \quad (14)$$

The relative inner generator's speed deviation will

also be examined in this article, a control signal to the FLCs, i.e. ($\omega_2 - \omega_4$) will be controlling TCBR1 and ($\omega_4 - \omega_2$) will be controlling TCBR2. Then the power that should be consumed via TCBR predicates on the deviation between the inner generator speed signals. Therefore, if $\omega_2 - \omega_4$ is positive then the $TCBR_1$ is energized if $\omega_4 - \omega_2$ is positive then the $TCBR_2$ is energized.

Gaussian and sigmoid fuzzy sets are chosen to interpret the MFs of the control variables of the FLC (for example the RKED in the p.u basis). The input MFs for the system are exhibited in Fig. 4. Three lingual variables, namely, PB (Positive Big), Z (Zero), and, NB (Negative Big) are defining the fuzziness of the FLC input. The MFs parameters implemented in this investigation are fixed and priorly selected via trial-and-error approach. The output type is constant having either 0 or 1 values (1 for PB, 0 for Z and NB). Where, 0 indicates that the TCBR should be fully OFF and 1 indicates that the TCBR should be fully ON. The same MFs are utilized for the other two control signal.

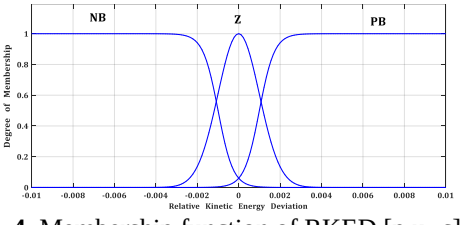

Fig. 4. Membership function of RKED [p.u.-s].

The propositioned braking scheme is direct and simple since it possesses three control rules only where the TCBR is inserted if the input exceeds a definite limit (i.e. the area has excess kinetic energy) and removed elsewhere (steady-state or the area has lack of the kinetic energy). There are three premise MFs in Fig. 4 and the conclusions are constants so the FLC rules are as follows. If the input is NB then the output is 0, if the input is Z then the output is 0, and if the input is PB then the output is 1. Then the triggering angle circuit will provide the necessary firing angle, α, pulses for the thyristors (for fuzzy output 0 then α=180 ^{o}, and for fuzzy output 1 then α=0

In the next section, nonlinear simulation studies are performed to highlight the capability of fuzzy controlled TCBRs to effectively alleviate the oscillations through ON-OFF (bang-bang) fuzzy-based control. This work will introduce the time responses of transmitted power as well as the relative generator speed responses for demonstrating the mitigation capability of the propositioned strategy.

The simulation studies are conducted via SimPower® of MATLAB™/Simulink. In what follows, five cases are performed to indicate the effectivity of the propositioned strategy for alleviation of the power oscillations. The considered case studies cover the changeability of a realistic power system contingencies. The non-linear 10-seconds simulation results are plotted and the responses of transmitted power from area (1) to area (2) without and with the propositioned alleviation strategy are compared to emphasize its capability of alleviating the power oscillations through ON-OFF (bang-bang) fuzzy-based control switching strategy.

4.1. Case study 1 — Momentarily Slight Increase in the Referenced Potential Setpoint of Generator (1)

In this case, the propositioned strategy is tested, under various energization signals, to alleviate the oscillations developed in the considered test grid to small disturbance. Under the considered stressed steady-state operating conditions, benchmark is provoked to encounter the inter-area mode of oscillation by having momentarily slight increase of 0.05 p.u. in setpoint of the reference potential of generator number (1) from 0.5 to 0.7 s. The sub curves detailed in the outline of Fig. 5 reflect the corresponding responses of inter-area real power transferred from area 1 to area 2 (P_{12}) and reactive power transferred from area 1 to area 2 (Q_{12}) of the benchmark as a consequent of the experienced small disturbance as measured at bus 7. Additionally, the relative generator speed responses are exhibited in the outline of Fig. 6 to manifest the oscillation behavior of the inter-area mode of oscillation.

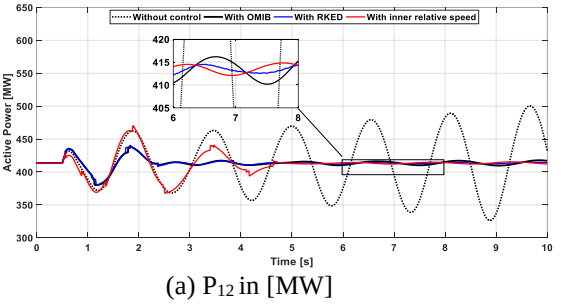

(a) P_{12} in [MW]

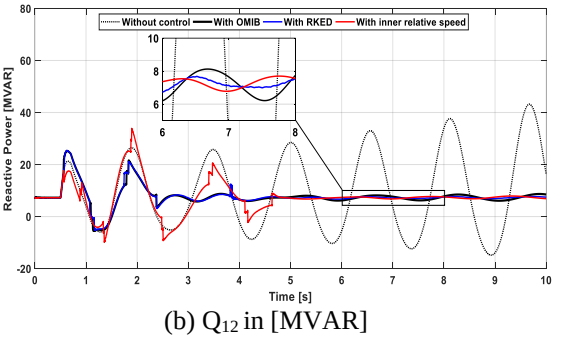

(b) Q_{12} in [MVAR]

Fig. 5. Transferred power responses to the small disturbance without and with resistor brake.

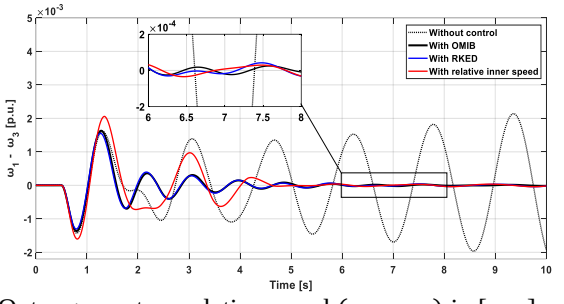

(a) Outer generators relative speed ($\omega_1 \_ \omega_3$) in [p.u.]

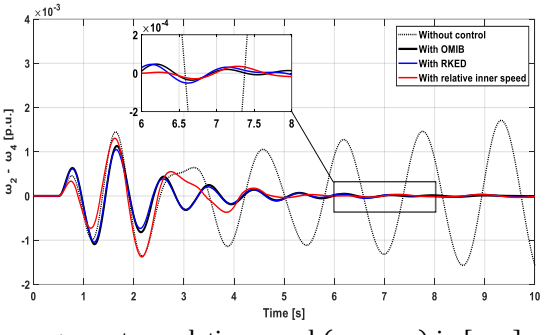

(b) Inner generators relative speed ($\omega_2 \_ \omega_4$) in [p.u.]

Fig. 6. Case (1) relative generator speeds time-domain responses.

From the earlier results, in the base-case plot (i.e. uncontrolled plot), the amplitudes of the power swing and relative speed responses are periodically increasing as the simulation period proceeds indicating the response instability feature. The protective relaying schemes shall respond to these unstable oscillations by taking tripping actions to the various system elements and then inevitably, whole grid will be fated to separate. It is seeable from the prior results, that the employment of TCBR significantly alleviate the speed and power oscillations. It also seems that the $OMIB_{speed}$, RKED, and the inner generators relative speed signals are effective in alleviating the developed oscillations. The TCBR alleviates the speed and power oscillations by absorbing the extra real power during the accelerating conditions. To elaborately elucidate the brake functioning, the responses of the TCBR real power dissipations in addition to the energization signals are exhibited in the figures from Figs. 7 to Fig. 9.

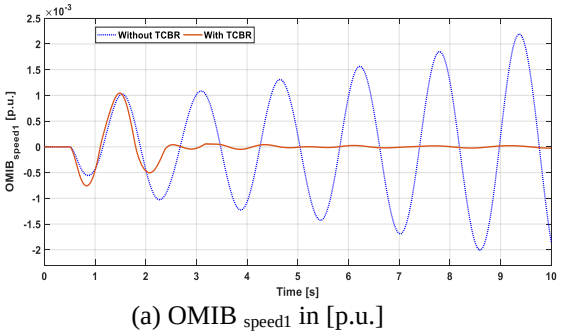

(a) OMIB $_{speed1}$ in [p.u.]

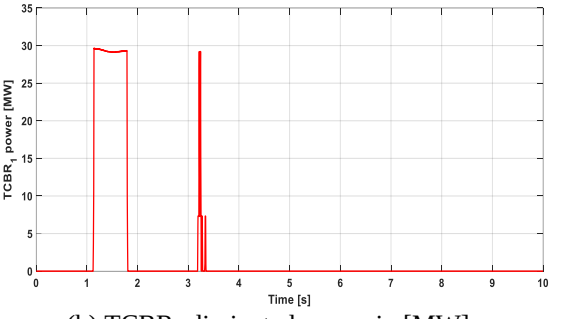

(b) $TCBR_1$ dissipated power in [MW]

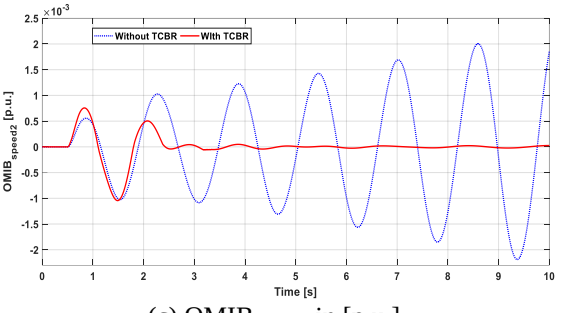

(c) OMIB $_{speed2}$ in [p.u.]

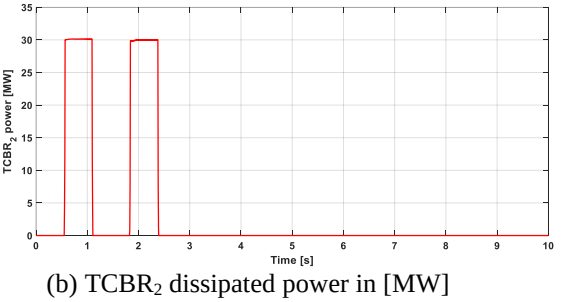

(b) $TCBR_2$ dissipated power in [MW]

Fig. 7., Case (1) $OMIB_{speed}$ and TCBR dissipated power responses.

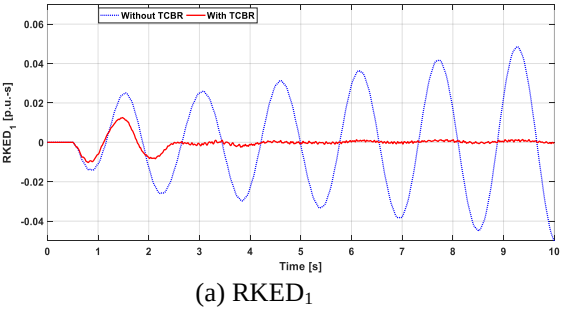

(a) $RKED_1$

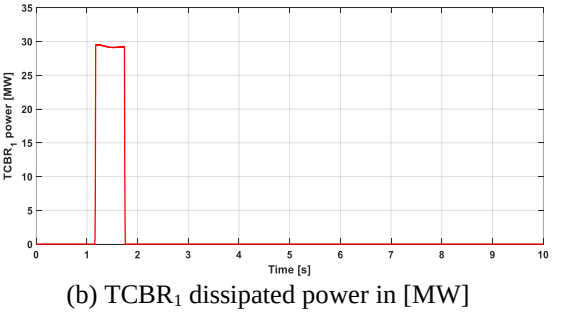

(b) $TCBR_1$ dissipated power in [MW]

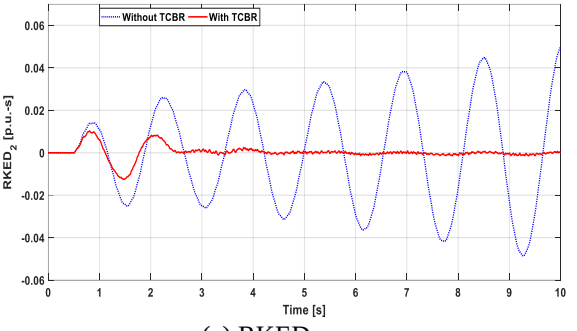

(c) $RKED_2$

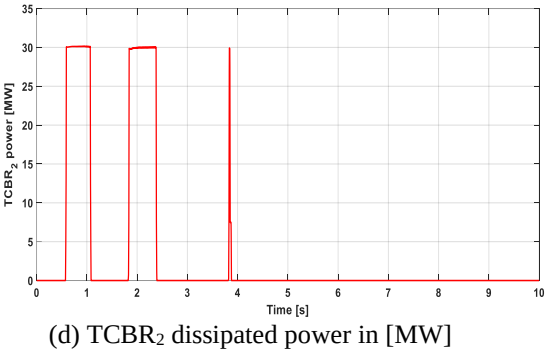

(d) $TCBR_2$ dissipated power in [MW]

Fig. 8. Case (1) RKED and TCBR power responses due to small step change in the referenced voltage of generator (1).

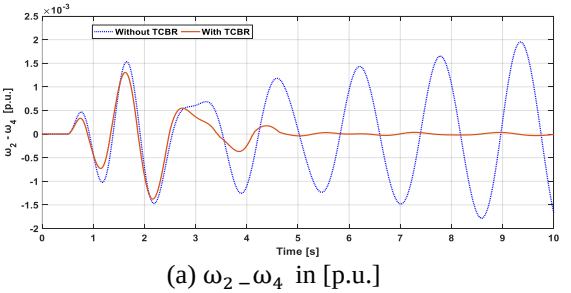

(a) $\omega_2 - \omega_4$ in [p.u.]

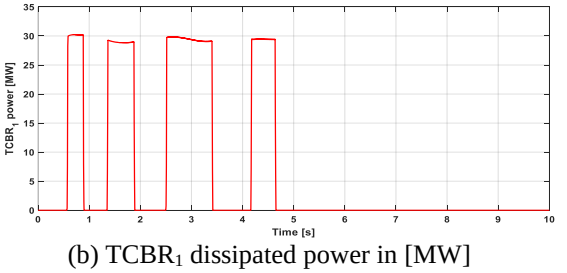

(b) $TCBR_1$ dissipated power in [MW]

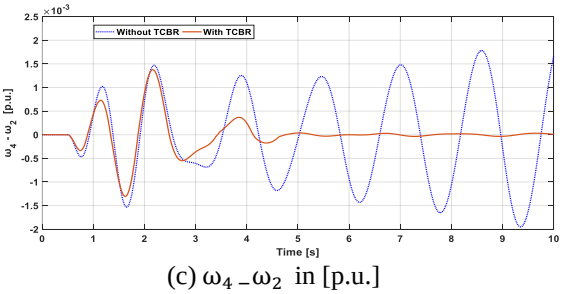

(c) $\omega_4 - \omega_2$ in [p.u.]

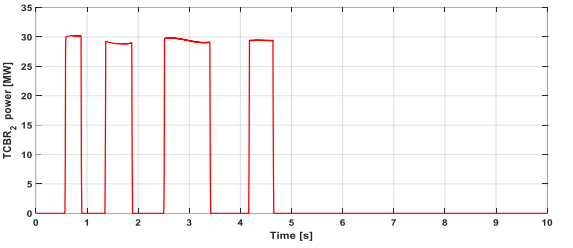

(d) $TCBR_2$ dissipated power in [MW]

Fig. 9. Case (1) relative inner speeds and TCBR dissipated power responses

It is evident from the previous results that both $OMIB_{speed}$ and RKED signals are leading to almost the same responses. Although, the relative inner generator's speed deviation signal leads to an enhanced response but with higher number of insertions of the associated brake.

4.2. Case study 2— Switching of Tie-Line (A)

In this case, the propositioned strategy is tested, under various energization signals, to mitigate inter area developed within the test grid to mild disturbance. Line switching is frequently recurring and unavoidable event in the power system's daily operation. Line switching is more frequent on a permanent basis than as an emergency e.g. to allow for the regular maintenance of the line. Refer to Fig. 3, the interconnecting tie-line (A) is switched off at t = 0.5 second from the simulation period. Plots for the reactive and real powers exported from area 1 to area 2 (as recorded on bus 7) without and with the fuzzy-based resistor braking interventions are introduced in Fig. 10.

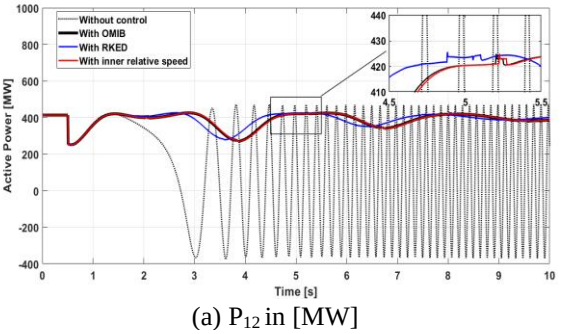

(a) P_{12} in [MW]

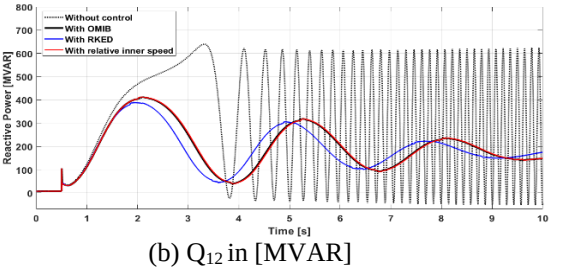

(b) Q_{12} in [MVAR]

Fig. 10. Transferred power responses to the switching of tie-line (A) without and with the dynamic brake.

It is obvious from the above responses that the switching of tie-line will cause an instantaneous reduction in the power output from the generators in area (1) and instantaneous reduction in the transmitted power to area (2) because both generators are now interconnected to area (2) via much weaker interface and the surplus electrical power which will not be transmitted to area (2) will be absorbed by the rotating masses of both generators in the kinetic energy form leading to the loss of synchronization in both areas. With the employment of the propositioned strategy, the benchmark maintains the synchronism state under the considered control signals. The responses of the TCBR real power dissipations accompanying the energization signals are exhibited in the figures from Fig.11 to Fig. 13.

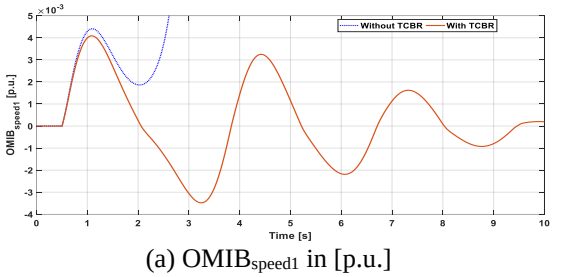

(a) $OMIB_{speed1}$ in [p.u.]

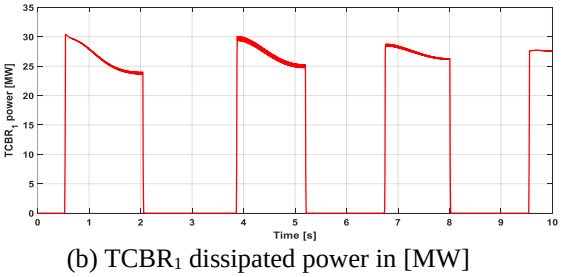

(b) $TCBR_1$ dissipated power in [MW]

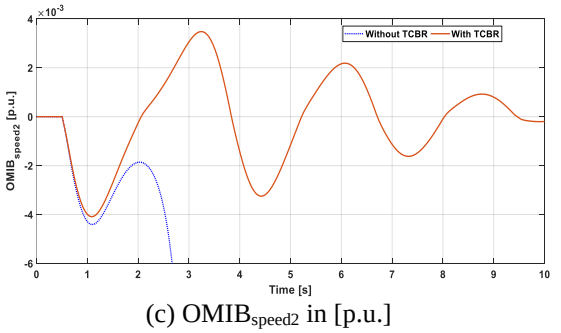

(c) $OMIB_{speed2}$ in [p.u.]

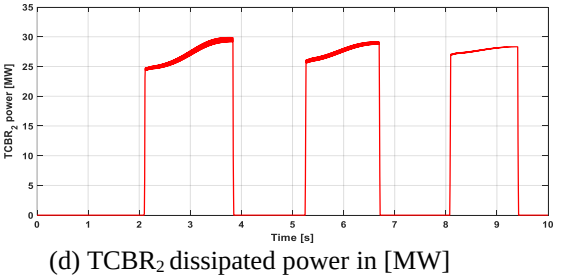

(d) $TCBR_2$ dissipated power in [MW]

Fig. 11. Case (2) $OMIB_{speed}$ and TCBR dissipated power responses.

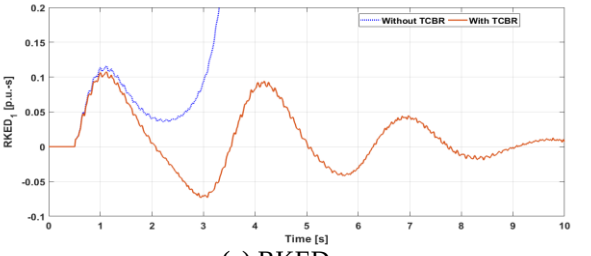

(a) $RKED_1$

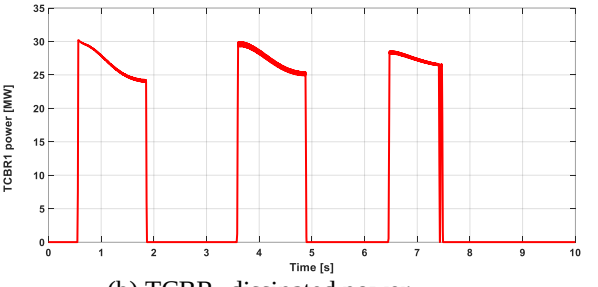

(b) $TCBR_1$ dissipated power

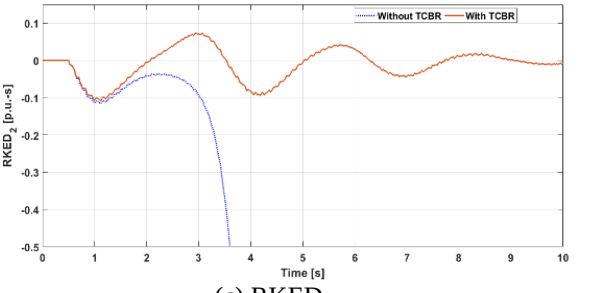

(c) $RKED_2$

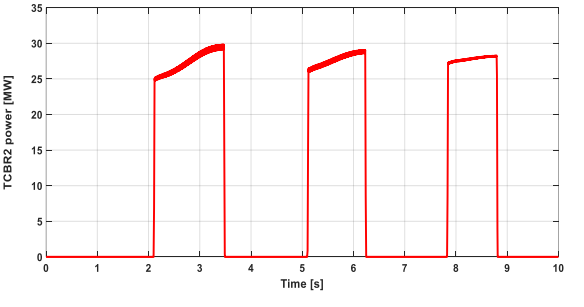

(d) $TCBR_2$ dissipated power in [MW]

Fig. 12. Case (2) RKED and TCBR power responses due to the switching of a tie-line.

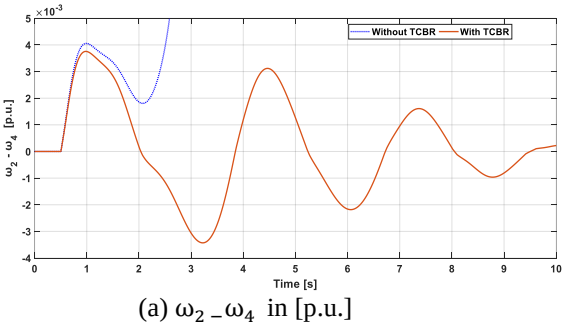

(a) $\omega_2 - \omega_4$ in [p.u.]

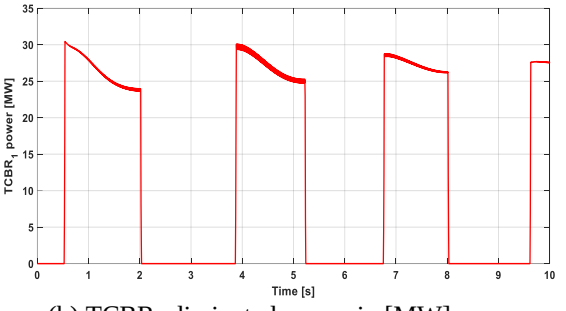

(b) $TCBR_1$ dissipated power in [MW]

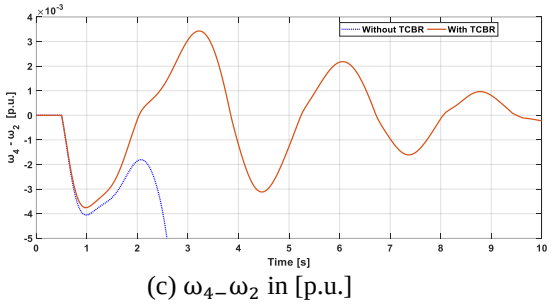

(c) $\omega_4 - \omega_2$ in [p.u.]

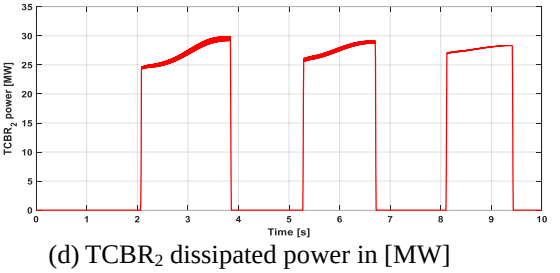

(d) $TCBR_2$ dissipated power in [MW]

Fig. 13. Case (2) relative inner speeds and TCBR and dissipated power responses.

It is evident from the above results that all control signals are leading to enhanced power profiles. Also, the results bear out that the implemented brake schemes lead to enhanced responses and protect the benchmark from losing its synchronism.

4.3. Case study 3 — 3LG Fault at the Mid of Tie-Line (A)

The propositioned strategy is tested herein, considering only RKED as an energization signal for brevity purposes, to alleviate inter area developed within the test grid to large disturbance. The transferred power responses are analyzed when the benchmark is subjected to three-phase permanent bolted three-phase to ground (3LG) fault, at the mid of the tie-line (A), at t = 0.5 s. The case scenario requests for 3 electrical cycles (~), or 50 ms from the disturbance initiation, to clear the disturbance by the simultaneous breaking of the circuit breakers (CBs) situated at the terminals of the tie-line (A). The simulation curves exhibited in Fig. 14 highlight comparative power transfer responses to this severe disturbance without and with the fuzzy-based resistive brake interventions considering the RKED only as an energization signal.

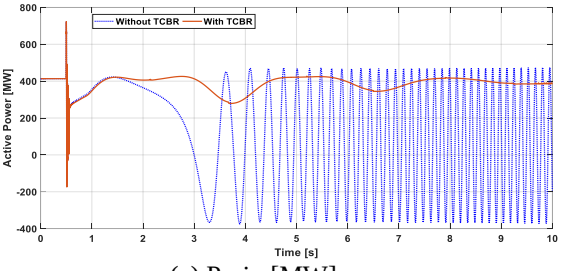

(a) P_{12} in [MW]

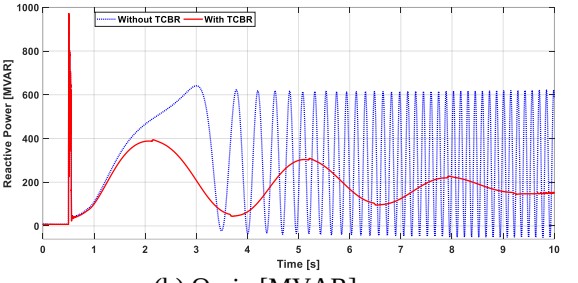

(b) Q_{12} in [MVAR]

Fig. 14. Transferred power responses due to 3LG at the mid of tie-line (A).

It is distinct from the transferred power responses that, the synchronism status is lost after about 3 s. By the employment of the propositioned strategy, the benchmark continues in the synchronism status in an adequate manner. Also, because of the employment of dual resistor brakes, the benchmark is sufficiently consolidated to get through this severe disturbance. The comparative RKED responses along with three-phase dissipated power in each resistor brake are introduced as a group of curves portrayed in the outline of Fig. 15.

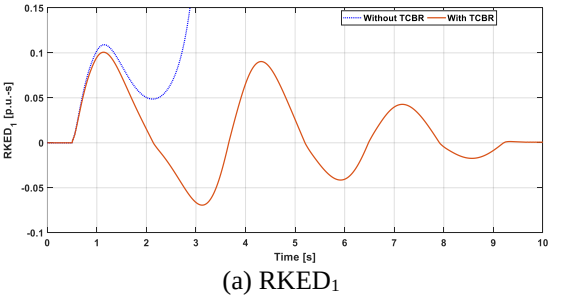

(a) $RKED_1$

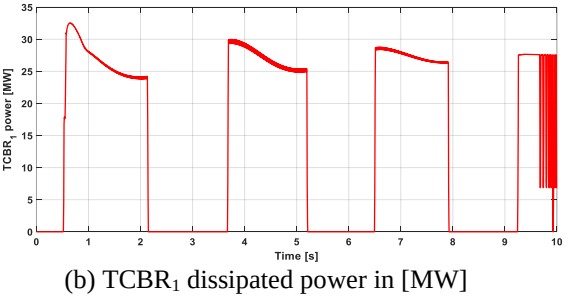

(b) $TCBR_1$ dissipated power in [MW]

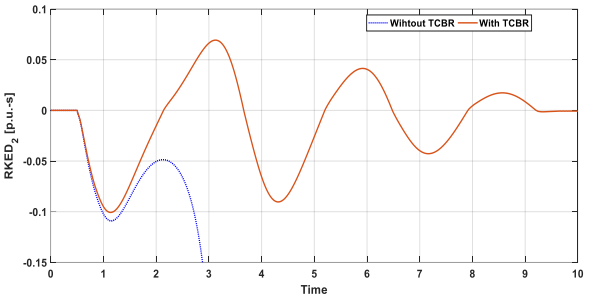

(c) $RKED_2$

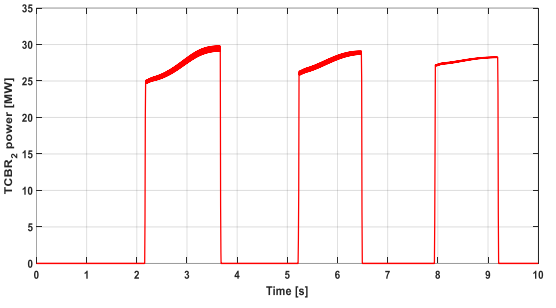

(d) $TCBR_2$ dissipated power in [MW].

Fig. 15. The comparative RKED responses along with three-phase dissipated power in each resistor brake.

It is distinctly noticed from the RKED responses that the benchmark loses synchronism without the employment of the propositioned alleviation strategy after about 3 s. With the employment of the propositioned strategy, the RKED responses of the benchmark will experience mitigated oscillatory behavior.

4.4. Case study 4 — l LG Fault with Successful Single Phase Autoreclosing

The propositioned strategy is tested herein, considering RKED as an energization signal, to mitigate inter area developed within the test grid to single phase to ground (1LG) fault followed by successful single phase autoreclosure. The transferred power responses are analysed when the benchmark is subjected to transient single-phase to ground fault at the phase (A) of the tie-line (A), at 0.5 s followed by single-phase successful autoreclosing of the CBs. The case scenario calls for clearing the perturbation in 3 ~ (50 ms) from the disturbance initiation by the simultaneous breaking of phase (A) of the CBs located at the terminals of the tie-line (A). Then the phase (A) of the CBs recloses simultaneously after 30 ~ (0.5 s) later. The curves introduced in Fig. 16 highlight the comparison of the transmitted power of the test grid to this disturbance.

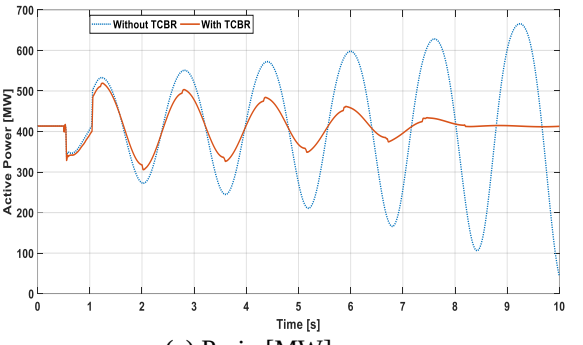

(a) P_{12} in [MW]

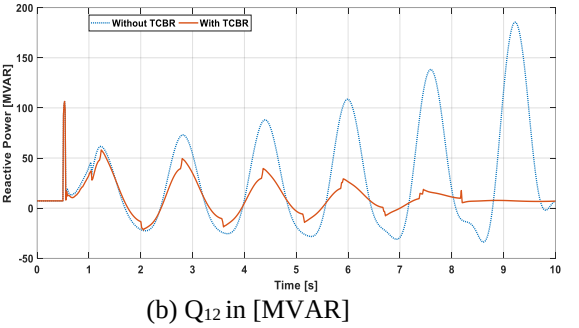

(b) Q_{12} in [MVAR]

Fig. 16. Transferred power responses to successful single-phase reclosure.

It is noticeable from the transferred power responses that, the benchmark is undergoing oscillation behavior with apparent negative damping which will ultimately lead to synchronism losing situation. By the employment of the propositioned strategy, the benchmark experiences a well-damped oscillation behavior. The comparative RKED responses along with three-phase dissipated power in each resistor brake are introduced as a group of curves exhibited in Fig. 22.

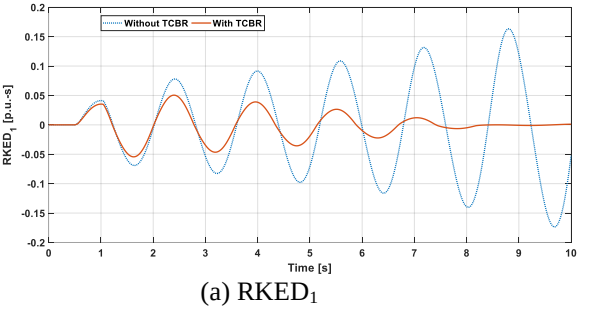

(a) $RKED_1$

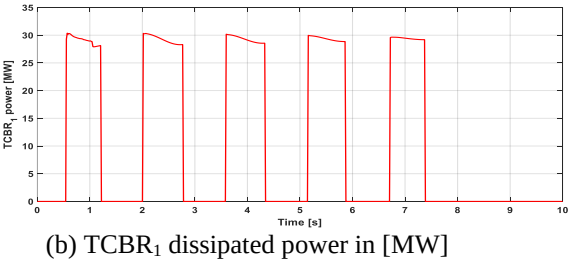

(b) $TCBR_1$ dissipated power in [MW]

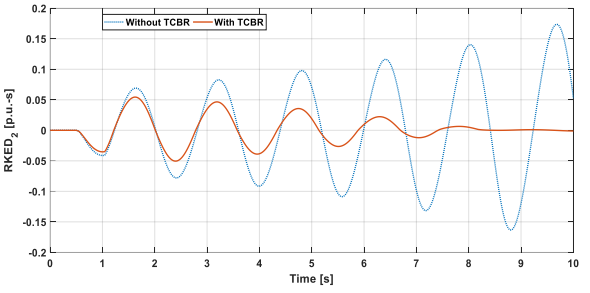

(c) $RKED_2$

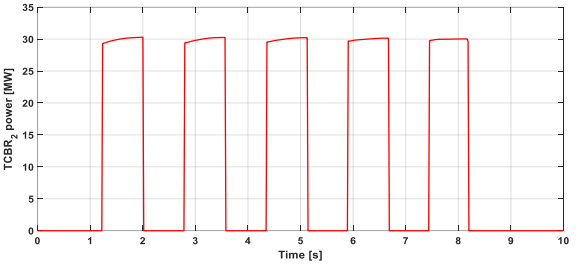

(d) $TCBR_2$ dissipated power in [MW]

Fig. 17. Case (6) RKED and TCBR dissipated power responses.

It is observable from Fig. 17 that after the balance between kinetic energies among the two power areas is restored, the benchmark oscillation behavior is alleviated. The $TCBR_1$ ceases to absorb active power after 7.38 s while $TCBR_2$ ceases to absorb active power after 8.2 s.

Case study 5 — Slight Increase in the Referenced Potential Setpoint of Generator (1) Considering Time latency

Number in real life power grids, a variable range of fixed time delays are included in the calculation of the RKED control signal. If the introduced time latency exceeded certain threshold value, the alleviation strategy could fail to provide the supplemental damping to inter area power oscillations. Therefore, the phenomenon time delay latency involved in online transmission of the RKED signal should be studied. Time latencies rely on many factors such as, the physical separation between the measuring device and the controller location, and the type of the communication channel used to transmit the signal. Accordingly, the introduced time delays are ranging several microseconds to few hundred milliseconds. There are many types of communication interfaces such as telephone lines, fiber-optic cables, microwave communication links, and satellites communication links [27]. The standard time delay ranges included in numerous communication links are tabularized in Table 1 [27]. Communication delays are not only associated with global centralized controllers, time latencies up to 50 ms should be considered in appraising the effectivity of local oscillation damping devices rather than neglecting them [28].

Table 1. Delays associated with various links.

Transmission interface	Time latency range
Fiber-optic cable	100-150 ms
Power line carrier	150-350 ms
Microwave	100-150 ms
Telephone lines	200-300 ms
Satellite link	up to 700 ms

In this case, a particular focus is devoted on testing the propositioned strategy in mitigation of the oscillations developed within the test grid to small disturbance when various time latencies are taken into consideration in the transmission of the energization signals to the resistive brake location (in this case only RKED is considered) from the different generators to the resistive brake location. The synchronous generator speed signals are transmitted to the TCBR location via a dedicated communication link and the RKED signal is calculated at the TCBR location to alleviate the potential inter-area power oscillations. Accordingly, case (1) is repeated with considering suitable time delays varying from 150 ms to 450 ms. The sub curves specified in the outline of Fig. 18 reflect the corresponding responses of power flows consequent to the experienced small disturbance. Additionally, the relative generator speed responses are exhibited in the outline of Fig. 19 to manifest the oscillation behavior of the inter-area mode of oscillation.

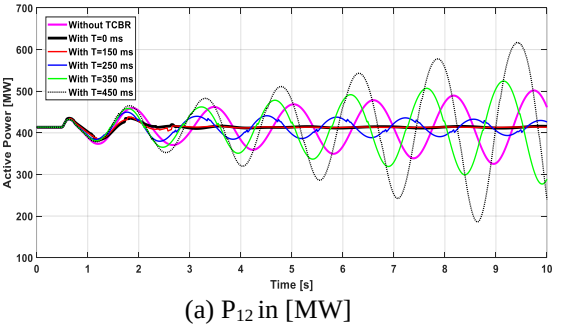

(a) P_{12} in [MW]

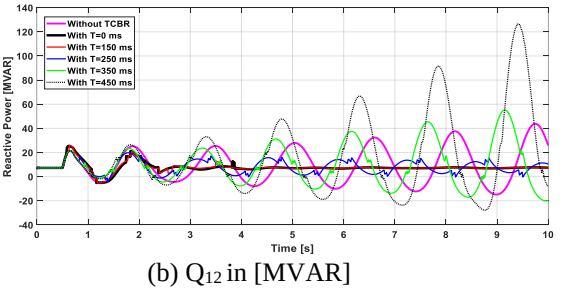

(b) Q_{12} in [MVAR]

Fig. 18. Transferred power responses to the small disturbance with time latencies

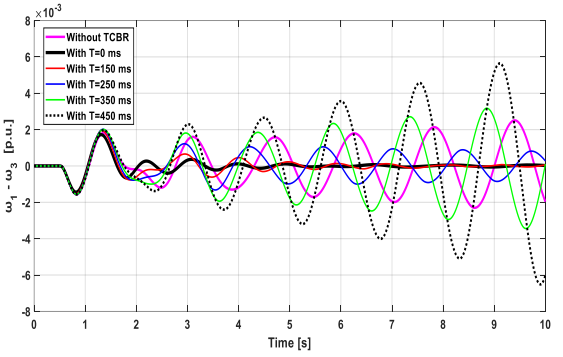

(a) Outer generators relative speed ($\omega_1 - \omega_3$) in [p.u.]

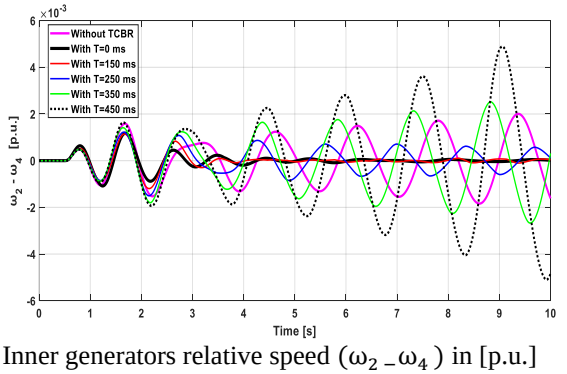

(b) Inner generators relative speed ($\omega_2 - \omega_4$) in [p.u.]

Fig. 19. Comparative relative outer and inner speeds to the small disturbance with time latencies.

It is apparent from the earlier results that time delays beyond certain threshold (Above 250 ms) has a destabilizing influence on power and speed deviation responses. Therefore, fiber optic communications links are very convenient from a practical perspective.

4.5. Case study 5— Slight Increase in the Referenced Potential Setpoint of Generator (1) Considering Declined Inertia

Recently, modern design tools and techniques accompanied with the technological accomplishments in the fields of metallurgy and composite materials and innovated cooling technologies have accomplished the designed power outputs from synchronous generators with reduced turbogenerator rotary shaft dimensions and more compact size [29]. Also, the electricity sector has witnessed escalated incursion levels of grid-connected photovoltaic plants [30]. As photovoltaic plants are being extensively implemented in an escalated manner substituting the conventional fossil fueled energy resources, the total grid inertia will keep decreasing. Therefore, the newly installed or replaced turbogenerator units will have declined inertia. In this last case study, the influence of the grid inertia declination on the mitigating capability of the propositioned strategy is studied. Accordingly, case (1) is repeated with considering that the inertia of each machine in area 1 reduction from its initial value of H = 6.5 seconds to 25% reduction i.e. H= 4.8750 seconds and to 50% reduction i.e. H= 3.25 seconds while the inertia of each machine in area 2 is held at the initial value. The sub curves grouped in the outline of Fig. 20, and Fig. 22 reflect the corresponding responses of power flows consequent to the experienced small disturbance considering 25% and 50% reductions in area (1) inertia, respectively. Additionally, the relative generator speed responses are detailed in the outline of Fig. 21 and Fig. 23 to manifest the oscillation behavior of the inter-area mode of oscillation.

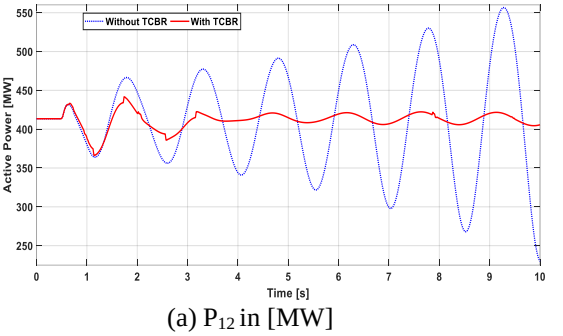

(a) P_{12} in [MW]

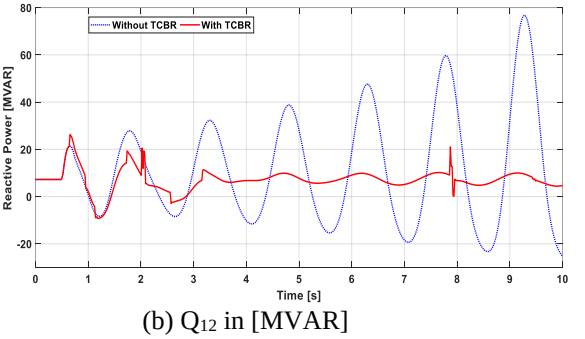

(b) Q_{12} in [MVAR]

Fig. 20. Transferred power responses considering 25% declined inertia in area (1).

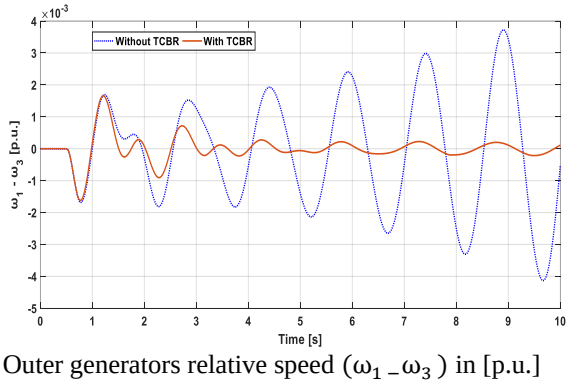

(a) Outer generators relative speed ($\omega_1 - \omega_3$) in [p.u.]

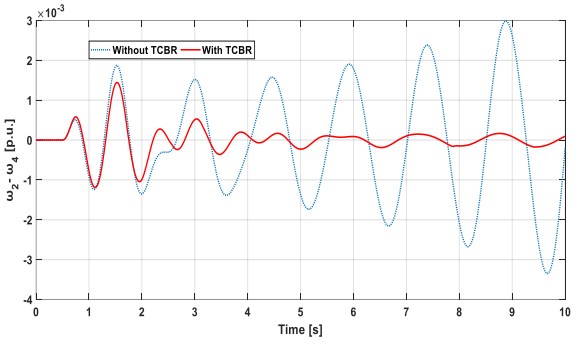

(b) Inner generators relative speed (ω_2 _ ω_4) in [p.u.]

Fig. 21. Comparative relative speeds to the small disturbance with 25% declined inertia in area (1).

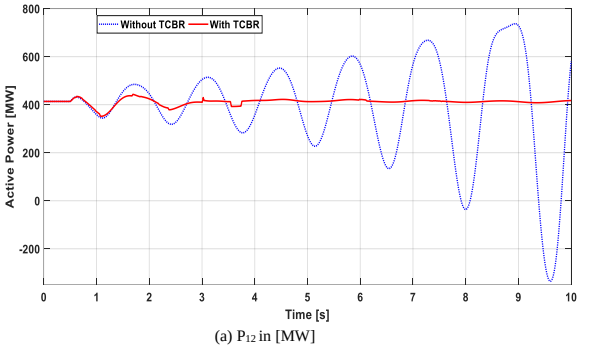

(a) P_{12} in [MW]

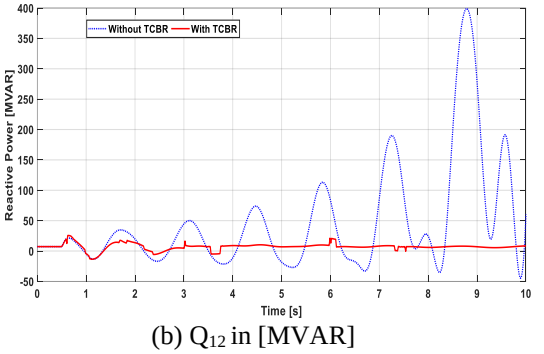

(b) Q_{12} in [MVAR]

Fig. 22. Transferred power responses to the small disturbance considering 50% reduced inertia.

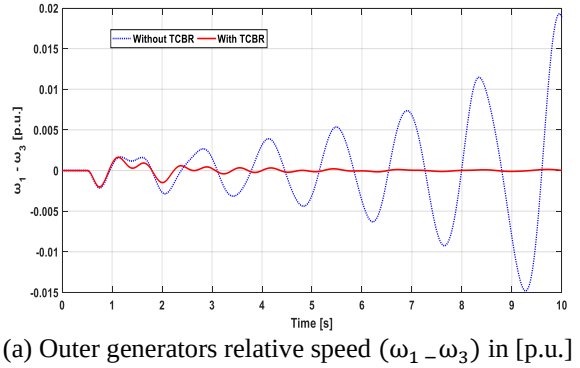

(a) Outer generators relative speed (ω_1 _ ω_3) in [p.u.]

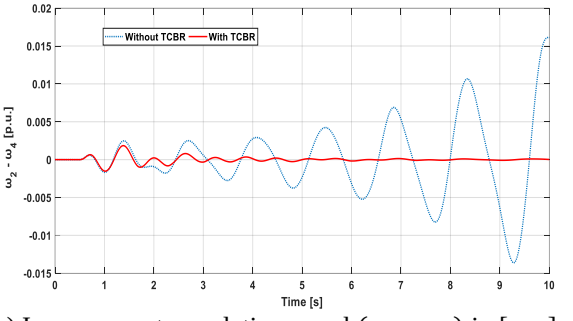

(b) Inner generators relative speed (ω_2 _ ω_4) in [p.u.]

Fig. 23. Comparative relative inner speeds to the small disturbance considering 50% reduced inertia.

From the above results, in the base-case plot, it is obviously noticed that both the oscillation amplitudes are increased as the benchmark inertia is declined which will shed some light on the inherent danger behind the escalated incursion levels of grid-connected photovoltaic plants as replacement for the conventional energy resources. With the employment of the propositioned strategy, the oscillation behavior is alleviated in an acceptable manner in both situations.

5. CONCLUSIONS

This article is proposing resistor brake scheme controlled via FLC to alleviate the encountered oscillation behavior as a direct outcome to the different grid perturbations. The propositioned strategy is tested on Kundur 4-machine 11-bus test systems. The key findings of this investigation are that the employment of dynamic resistive brake is providing excellent supplemental damping to poorly damped oscillation behavior manifested under stressful operating conditions. Moreover, the propositioned fuzzy strategy is differentiated by its simpleness since only three fuzzy rules involved in the decision-making procedures which decreases the computational burdens related to in real world implementations. In summary, the simulation curves within this investigation give a good impression on the potential of the propositioned strategy, as a relatively cost-effective countermeasure, with regard to the neutralizing of inter area power and relative speed oscillations. Therefore, the employment of the propositioned strategy will make power grids less vulnerable to the tedious problems of unstable power oscillations with the consequent chain reaction power outage failures.

6. APPENDEX

Refer to Fig. 3, the Kundur synchronous generators' dynamic data in p.u. based on 900 MVA as a base power and 20 kV as a base voltage are tabularized in

Table A. 1. Kundur 20 kV transmission system' electrical data are tabularized in [7].

Table A.1. Turbogenerator shaft detailed parameters.

No. of Generator	**1 & 2**	**3 &4**
Rotor type	Round Rotor	Round Rotor
Inertia constant H	6.5 s	6.175
Stator resistance R_a	0.0025 p.u.	0.0025 p.u.
Leakage reactance X_l	0.2 p.u.	0.2 p.u.
Synchronous reactance x_d	1.8 p.u.	1.8 p.u.
Synchronous reactance x_q	1.7 p.u.	1.7 p.u.
Transient reactance x_d'	0.3 p.u.	0.3 p.u.
Transient reactance x_q'	0.55 p.u.	0.55 p.u.
Subtransient reactance x_d''	0.25 p.u.	0.25 p.u.
Subtransient reactance x_q''	0.25 p.u.	0.25 p.u.
Transient time constant T_{d0}'	8 s	8 s
Transient time constant T_{q0}'	0.4 s	0.4 s
Subtransient time constant T_{d0}''	0.03 s	0.03 s
Subtransient time constant T_{q0}''	0.05 s	0.05 s

REFERENCES

[1] G. Rogers, **:"Power system oscillations",** *New York: Springer-Verlag Inc*, 2000.

[2] L. L. Grigsby, **"Power system stability and control",** *Bosa Roca: CRC Press Inc*, 2012.

[3] S. You, G. Kou, Y. Liu, X. Zhang, Y. Cui, M. J. Till, W. Yao, and Y. Liu, **"Impact of high PV penetration on the inter-area oscillations in the U.S. Eastern Interconnection,"** *IEEE Access*, Vol. 5, pp. 4361-4369, 2017. https://doi.org/10.1109/ACCESS.2017.2682260.

[4] Y. Cui, L. Wu, W. Yu, Y. Liu, W. Yao, D. Zhou, and Y. Liu, **"Inter-area oscillation statistical analysis of the U.S. Eastern Interconnection,"** *The J. Engineering*, Vol. 11, pp. 595 – 605, 2017. https://doi.org/10.1049/joe.2017.0243.

[5] D. P. Wadduwage, U. D. Annakkage, and K. Narendra, **"Identification of dominant low-frequency modes in ring-down oscillations using multiple Prony models,"** *IET Gener. Trans. & Distribu.*, Vol. 15, pp. 2206 – 2214, 2015. https://doi.org/10.1049/iet-gtd.2014.0947.

[6] F. K. A. Lami, **"A new improved method to damp inter-area oscillations in power systems with SSR mitigation and zone protection compensation",** *Ph.D. Thesis, University of Leicester, Leicester, United Kingdom*. 2012.

[7] M. Hadjikypris, **"Supervisory control scheme for FACTS and HVDC based damping of inter-area power oscillations in hybrid ac-dc power systems",** *Ph.D. Thesis, University of Manchester, Manchester, United Kingdom*, 2015.

[8] P. Kundur, **"Power system stability and control",** *New York: McGraw-Hill Inc*, 1994.

[9] E D. F. Peelo, D. W. Hein, and F. Peretti, **"Application of a 138 kV 200 MW braking resistor,"** *Power Engineering Journal*, Vol. 84, pp. 188-192, 1994. http://dx.doi.org/10.1049/pe:19940408.

[10] M. L. Shelton, W. A. Mittelstadt, P. F. Winkelman, and W. J. Bellerby, **"Bonneville power administration 1400 MW braking resistor,"** *IEEE Trans. Power Apparat. Syst.*, Vol. 94, pp. 602-611, 1975. https://doi.org/10.1109/T-PAS.1975.31888.

[11] R. Preece**, "Improving the stability of meshed power networks: a probabilistic approach using embedded HVDC lines".** *Cham: Springer International Publishing AG*, 2013.

[12] M. F. Ahmed, M. A. Mandor, M. El-Hadidy, and F. M. Bendary, **"Fuzzy based battery energy storage system and braking resistor for mitigation of shaft-torsional oscillations,"** *J. King Saud Univ. – Eng. Sci*, in press, 2020, https://doi.org/10.1016/j.jksues.2020.07.011.

[13] R. M. Hamouda, **"Damping torsional oscillations using thyristor controlled braking resistors,"** *J. King Saud Univ. – Eng. Sci.* Vol. 13, pp. 103-116, 2001. https://doi.org/10.1016/S1018-3639(18)30728-1.

[14] H. M. A. Rahim, **"A minimum-time based fuzzy logic dynamic braking resistor control for sub-synchronous resonance,"** *Electrical Power and Energy Systems*, Vol. 26, pp. 191–198, 2004. https://doi.org/10.1016/j.ijepes.2003.10.011.

[15] M. H. Ali, T. Murata, and J. Tamura, **"The effect of temperature rise of the fuzzy controlled braking resistors on transient stability,"** *IEEE Trans. Power Syst.*, vol. 19, pp. 1085-1095. 2004. https://doi.org/10.1109/TPWRS.2004.825828.

[16] M. H. Ali, T. Murata, and J. Tamura, **"Effect of coordination of optimal reclosing and fuzzy controlled braking resistor on transient stability during unsuccessful reclosing,"** *IEEE Trans. Power Syst.*, Vol. 21, pp. 1321- 1330, 2006, https://doi.org/10.1109/TPWRS.2006.876670.

[17] M. H. Ali, T. Murata, and J. Tamura, **"Influence of communication delay on the performance of fuzzy logic-controlled braking resistor against transient stability,"** *IEEE Trans. Control Syst. Technol.*, Vol. 16, pp. 1232-1241, 2008. https://doi.org/10.1109/TCST.2008.919443.

[18] T. Hiyama, M. Mishiro, and H. Kihara, **"Fuzzy logic switching of thyristor controlled braking resistor considering coordination with SVC,"** *IEEE Trans. Power Deliv.*, Vol. 10, pp. 2020-2026, 1995. https://doi.org/10.110961.473348.

[19] M. Glavic, **"Design of a resistive brake controller**

for power system stability enhancement using reinforcement learning," *IEEE Trans. Control Syst. Technol.*, Vol. 13, pp. 743- 751, 2005. https://doi.org/10.1109/TCST. 2005.847339.

[20] F. Ishiguro, S. Tanaka, M. Shimomura, T. Maeda, K. Matsushita, and H. Sugimoto, **"Coordinated stabilizing control of exciter, turbine and braking resistor,"** *IEEE Trans. Power Syst*. Vol. 1, pp. 74-80, 1986. https://doi.org/10.1109/TPWRS. 1986.4334957.

[21] S. M. Muyeen, **"A combined approach of using an SDBR and a STATCOM to enhance the stability of a wind farm,"** *IEEE Syst. Journal*, Vol. 9, pp. 922-932, 2014. https://doi.org/10.1109/JSYST. 2013.2297180.

[22] J. Mendel, H. Hagras, W. W. Tan, W. W. Melek, and H. Ying, **"Introduction to type-2 fuzzy logic control: theory and applications",** *New York: John Wiley & Sons Inc*, 2013.

[23] H. Altaş, **"Fuzzy logic control in energy systems with design applications",** *Stevenage: Institution of Engineering & Technology*, 2017.

[24] O. Castillo, and P. Melin, **"Type-2 fuzzy logic: theory and applications",** *Berlin: Springer-Verlag*, 2008.

[25] M. Klein, G. J. Rogers, and P. Kundur, **"A fundamental study of inter-area oscillations in power systems,"** *IEEE Trans. Power Syst.*, Vol. 6 3, pp. 914–921, https://doi.org/10.1109/59.119229

[26] E. Huseinbasic, I. Kuzle, and T. Tomisa, **"Inter-area oscillations damping using dynamic braking and phasor measurements,"** *IEEE/PES Power Systems Conference and Exposition*, pp. 1 – 6, 2009, https://doi.org/10.1109/PSCE.2009.4840068.

[27] S. Islam, P. X. Liu, and A. El Saddik, **"Wide-area measurement-based power system for smart transmission grid with communication delay,"** *IEEE International Instrumentation and Measurement Technology Conference (I2MTC)*, pp. 138-143, 2012. https://doi.org/10.1109/I2MTC.2012.6229458.

[28] T. Surinkaew, and I. Ngamroo, **"Inter area oscillation damping control design considering impact of variable latencies,"** *IEEE Trans. Power Syst.*, Vol. 34, pp. 481-493, 2019. https://doi.org/10.1109/TPWRS.2018.2866032.

[29] J. Bladh, P. Sundqvist, and U. Lundin, **"Torsional stability of hydropower units under influence of subsynchronous oscillations,"** *IEEE Trans. Power Syst.*, Vol. 284, pp. 3826-3833, 2013, https://doi.org/10.1109/TPWRS.2013.2263811.

[30] P. S. Sikder, and N. Pal, **"Modeling of an intelligent battery controller for standalone solar-wind hybrid distributed generation system,"** *J. King Saud Univ. – Eng. Sci*, in press, 2019. https://doi.org/10.1016/j.jksues.2019.02.002.